SUPPORTING INFORMATION FOR

Resolving the Enthalpy of Protein Stabilization by Macromolecular Crowding

Claire J. Stewart,[1§] Gil I. Olgenblum,[2§] Ashlee Propst,[1] Daniel Harries[2,*] and Gary J. Pielak[1,*]

[1]*Department of Chemistry, University of North Carolina at Chapel Hill, Chapel Hill, NC, 27599-3290, USA.*
[2]*Institute of Chemistry & the Fritz Haber Research Center, The Hebrew University, Jerusalem, Israel 91904*

[§] C.J.S and G.I.O contributed equally.

* gary_pielak@unc.edu, daniel.harries@mail.huji.ac.il

Materials and Methods

Cosolutes. PEGs were purchased from Sigma-Aldrich and ethylene glycol from Thermo Fisher. Solutions were prepared to the desired concentration in NMR buffer (50 mM $NaPO_4$,, 50 mM NaCl, 5% D_2O, pH 7.5). The pH was adjusted to 7.5 using concentrated HCl or NaOH.

Protein expression and purification. WT SH3 labeled with 5-fluorotryptophan was expressed and purified as described (Gorensek-Benitez et al. 2017; Stadmiller et al. 2017; Stadmiller et al. 2018; Thole et al. 2021), except that expression was allowed to proceed for 12−16 h at 18.5 °C.

^{19}F NMR. Samples were resuspended in either NMR buffer or NMR buffer containing desired amount of PEG. Experiments were performed at temperatures of 283 K, 288 K, 293 K, 298 K, 303 K, 308 K, 313 K, and 318 K to determine the temperature-dependance of stability. The magnet used was a Bruker Avance III HD spectrometer operating at a ^{19}F Larmor frequency of 470 MHz equipped with a cryogenic QCI probe. Experiments were acquired with a total relaxation delay of 2 s, a sweep width of 20 ppm, and a transmitter frequency offset of -124 ppm.

Data processing and analysis. NMR data were analyzed in Topspin 3.6.1 (Bruker), as described (Senske et al. 2016; Smith et al. 2016; Stadmiller et al. 2017). Spectra were indirectly (^{19}F) referenced to DSS (Maurer et al. 1996; Stadmiller et al. 2017). Further analysis was performed using MATLAB. Spectra were processed with a 5 Hz exponential line broadening function. R2017b, the integrated Gibbs-Helmholtz equation and Kirchhoff's equations (Senske et al. 2016).

Experiment-Derived Results

Entropy of unfolding. The free energy of unfolding (Fig. 1C) can be broken down the enthalpic (Fig. 1D) and entropic components (Fig. S1). These components almost cancel each other, leaving a marginally stabilizing effect.

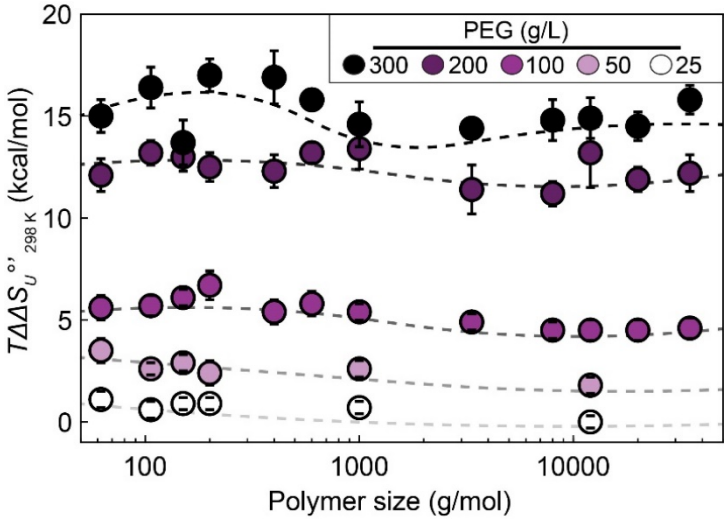

Figure S1. The energetic component of the entropy of SH3 unfolding as a function of PEG molecular weight and concentration ($T\Delta\Delta S^{\circ'}_{U} = T\Delta S^{\circ'}_{U,\mathrm{crowder}} - T\Delta S^{\circ'}_{U,\mathrm{buffer}}$) Color intensity increases with PEG concentration. Error bars denote the standard deviation of the mean from triplicate experiments and error propagation. Smooth curves are an aid to the eye and are of no theoretical significance.

Heat capacity of unfolding. The unfolding thermodynamics of WT SH3 were fitted using the integrated Gibbs-Helmholtz equation (see main text). The resulting denaturation heat capacities, $\Delta C_P^{\circ'}$, are shown in Fig. S2. $\Delta C_P^{\circ'}$ is constant as a function of PEG size, with a marked increase in the standard deviation with increasing concentration.

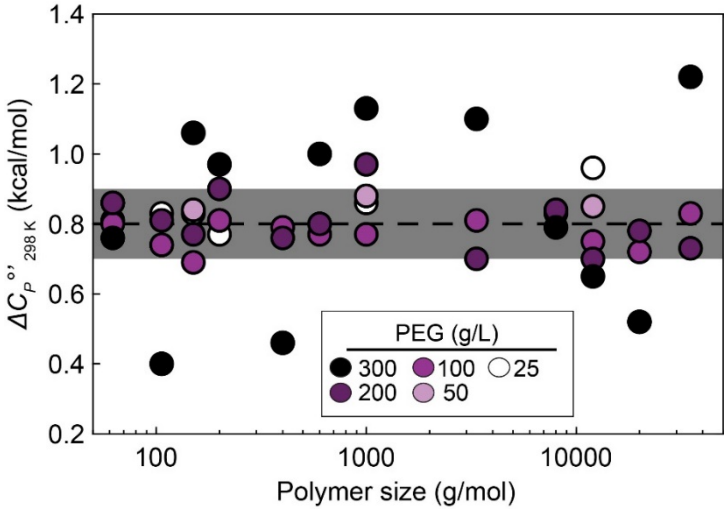

Figure S2. Change in heat capacity for each PEG solution determined from fit to the integrated Gibbs-Helmholtz equation. Dashed line is the average and gray box denotes the points within one standard deviation of the buffer value.

m-values. Values in Fig. 1E and F of the main text are calculated from the slope of the fits in Fig. S3. Deviation from linearity is observed for small PEGs. Those fits were truncated at 1M.

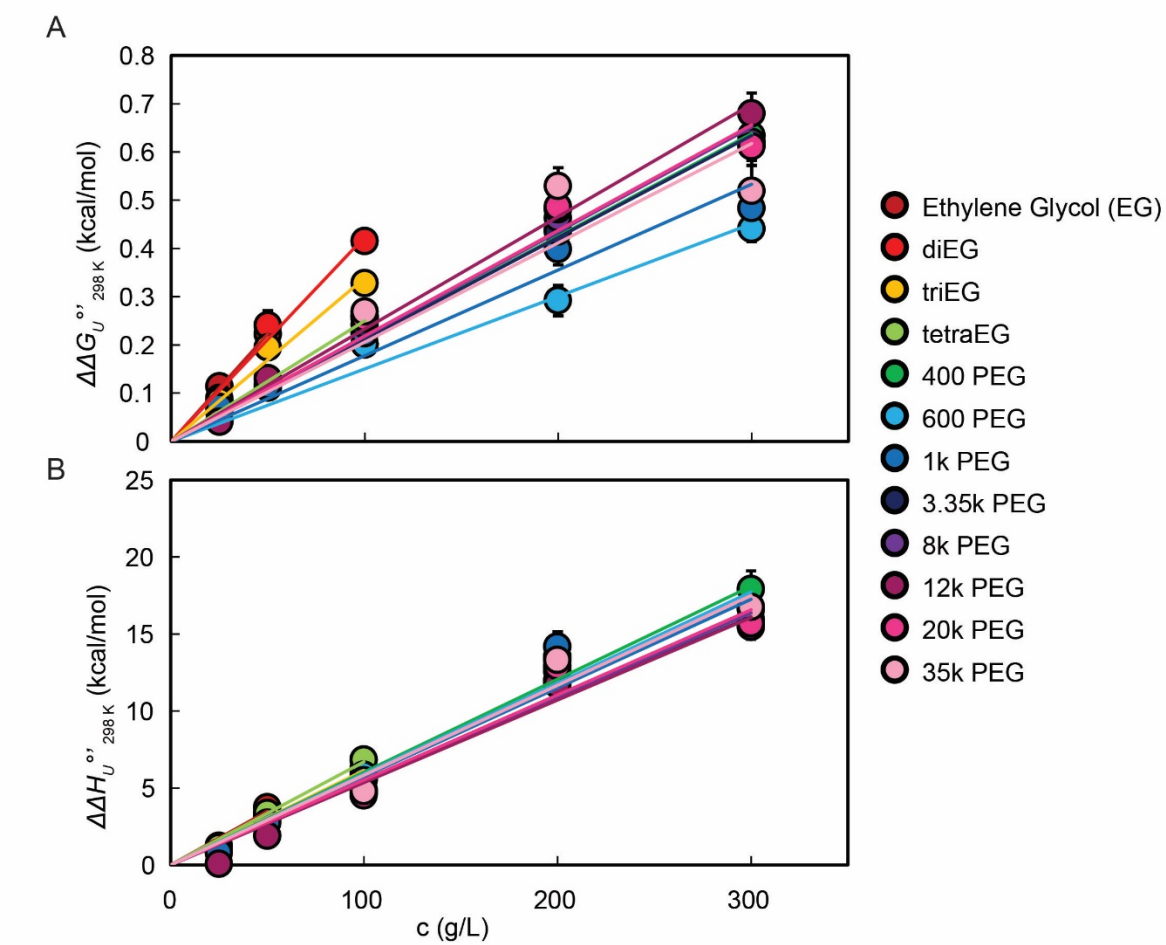

Figure S3. Linear fits of (A) stability and (B) enthalpy of SH3 unfolding against PEG concentration (g/L). The slopes represent *m*-values. Error bars denote the standard deviation of the mean from triplicate experiments.

^{19}F chemical shift perturbation. The chemical shift perturbation for the folded state is much greater that than for the unfolded states (Fig. 2B and Table S2) indicating an increase in interactions between folded SH3 and the small PEGs. Increasing PEG concentration increases the chemical shift perturbation for both states (Fig. S4), and the small PEGs have the greatest effects.

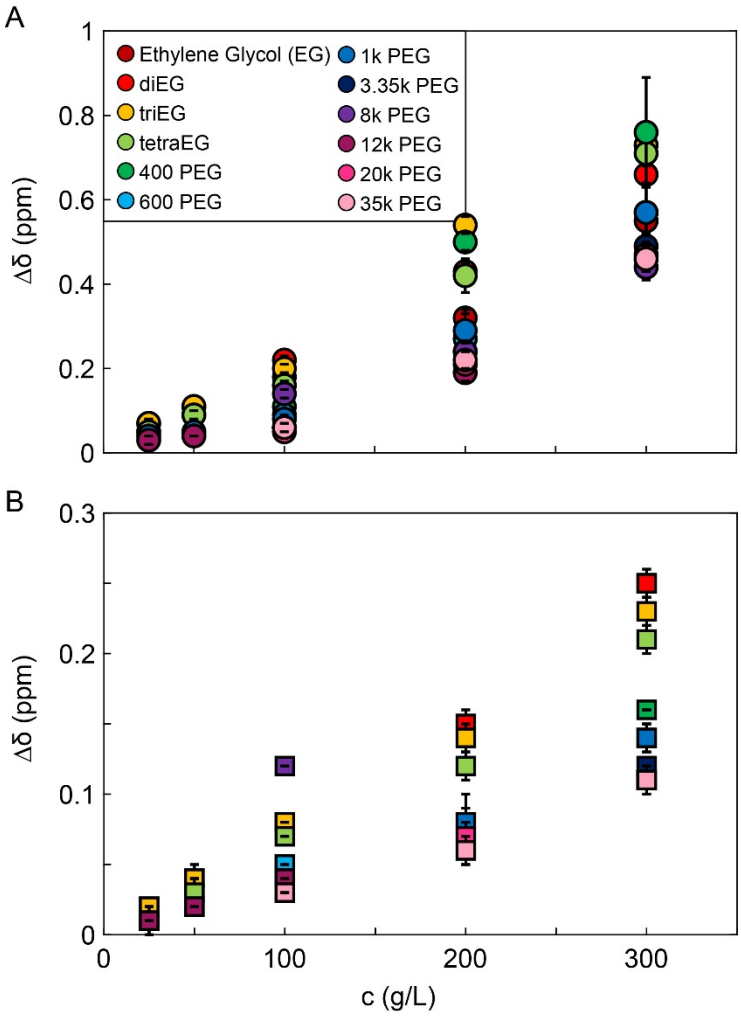

Figure S4. The change in ^{19}F chemical shift as a function of concentration for the folded (**A**) and unfolded (**B**) states. Error bars denote the standard deviation of the mean from triplicate experiments.

Crowding and the unfolded state. We use a mean-field model based on regular-solution theory and divide the system into a bulk domain and a protein surface domain. Both contain molecularly small solvent molecules (water), and larger cosolute molecules. We follow the Flory-Huggins (FH) approximation for the free energy of binary mixtures that considers solvent and cosolute of different molecular sizes. In the bulk domain, the FH mixing free energy is given by:

$$\frac{\beta \Delta G_{bulk}}{V_b} = \phi_S \ln \phi_S + \frac{\phi_C}{\nu} \ln \phi_C + \chi \phi_S \phi_C \tag{S1}$$

In Eq. (S1), $\beta = \left(kT\right)^{-1}$ where k is Boltzmann's constant, T is absolute temperature, ϕ_S and ϕ_C are the volume fractions of solvent and cosolute, respectively. V_b is the bulk volume in units of water molecular volume, $\bar{V}_s = a_s{}^3$; a_s is a water molecule linear length scale. ν is the ratio of cosolute to water partial molar volumes ($\bar{V}_C / \bar{V}_S$), and χ is the FH mixing parameter, which has enthalpic and entropic components, $\chi = \chi_H - \chi_{HS}$. Attractive and repulsive solvent-cosolute interactions correspond to negative and positive χ values, respectively. Although χ is typically reported using kT units, it can also be presented in units of $kcal / L$ (Table. S5).

For the protein surface domain, we modify the mixing entropy by rescaling the concentration to account for the smaller mixing volume near the protein surface (Sapir et al. 2015).

$$\begin{aligned} V_{surf} &= \Delta SASA \cdot a \\ V_{mix} &= V_{surf} \left[1 - \frac{1}{2} \left(1 - \frac{1}{a} \right) \left(1 - \phi_C^{surf} \right) \right] \\ \phi_C^{mix} &= \phi_C^{surf} \frac{V_{surf}}{V_{mix}} \\ \phi_S^{mix} &= 1 - \phi_C^{mix} \end{aligned} \tag{S2}$$

In Eq. (S2) V_{mix} and V_{surf} are the rescaled and non-rescaled volumes at the surface. ϕ_C^{surf} and ϕ_C^{mix} are the corresponding rescaled and non-rescaled cosolute volume fractions, and ϕ_S^{mix} is the rescaled solvent volume fraction in the protein surface domain. a is the surface domain thickness, i.e., the linear dimension of the cosolute molecule (Fig. 3A of the main text). $\Delta SASA$ is the solvent accessible surface area ($SASA$) of the unfolded state minus the $SASA$ of the folded state. Marsh et al. used NMR data to show that this SH3 has a compact unfolded state (Marsh et al. 2007), and we use their $\Delta SASA$ value of 2200 Å^2, which is derived from an ensemble of unfolded structures. This value is less than the estimate for a fully unfolded protein because SH3 has a compact unfolded ensemble. We add a surface-cosolute chemical interaction term, ε, to arrive at the following mixing free energy (ΔG_{surf}) at the protein surface domain:

$$\beta \Delta G_{surf} = V_{mix} \left[\phi_S{}^{mix} \ln \phi_S^{mix} + \frac{1}{\nu} \phi_C^{mix} \ln \phi_C^{mix} \right] + \chi_{surf} V_{surf} \phi_S^{surf} \phi_C^{surf} + \frac{\varepsilon}{a} V_{surf} \phi_C^{surf} \tag{S3}$$

Where ε is in kT / a_s^2 units, (but can also be reported in units of $kcal \cdot mol^{-1} \cdot nm^{-2}$, Table. S6).

From the bulk and surface free energies, we calculate the chemical potential, μ, of the *i*-th component (cosolute – C or solvent – S) as the derivative of the free energy with respect to the total number of molecules of that component, N_i, so that

$$\mu_i^{surf/bulk} = \left(\frac{\partial \Delta G_{surf/bulk}}{\partial N_i} \right)_{\beta, N_{j \neq i}} \tag{S4}$$

These chemical potentials are used to numerically solve for the equilibrium condition,

$$\mu_C^{surf} - \nu \mu_S^{surf} - \mu_C^{bulk} + \nu \mu_S^{bulk} = 0 \tag{S5}$$

We extract the parameters used in these expressions by fitting experiment-based results, thus dissecting the contribution to the free energy originating from the excluded volume effect, solvent-cosolute interactions, and cosolute-protein interactions through the parameters, ν, χ and ε, respectively. Note that ν and χ depend on cosolute and solvent but are independent of the protein.

Adsorption to the folded state. For the folded state free energy change, we use a model that considers displacement of water from, and adsorption of cosolute molecules to, specific binding sites (Fig. 3A). We begin with a solution comprising M, N_S, and N_C, protein, solvent, and cosolute molecules, respectively. We assume that each protein has m adsorption sites occupied by either water or cosolute. Specifically, the simple case of a single adsorption site on each protein, $m = 1$, results in the Langmuir-like adsorption isotherm. We then define a partition function that accounts for the equilibrium involving displacement of water from and adsorption of cosolute molecules to a protein adsorption site:

$$q(i) = e^{-\frac{\Delta g(i)}{kT}} \tag{S6}$$

where $\Delta g(i) = \Delta h(i) - T\Delta s(i)$ is the free energy, internal energy, and entropy associated with adsorption of i cosolute molecules, presented in terms of $kcal/mol$ or kT per binding site (i.e., unitless, Table. S6).

This system's canonical partition function is:

$$Q(M, N_W, N_S, V, T) = \sum_b \frac{q(0)^{b_0} q(1)^{b_1} \cdots q(m)^{b_m}}{b_0! b_1! \cdots b_m!} \tag{S7}$$

where b_i is the number of proteins with i cosolute molecules adsorbed, and the sum over all values from b_0 (only water adsorbed) to b_m (only cosolute adsorbed).

We next write the grand canonical partition function,

$$\Gamma\left(M\ ,V,\mu_W,\mu_S\right)=\sum_{N_S}^{mM}\sum_{N_W}^{mM}Q\lambda_W^{N_W}\lambda_S^{N_S} \tag{S8}$$

where $\lambda_{S/C}=\exp\left(\beta\mu_{S/C}^{bulk}\right)$. For the bulk chemical potentials we use the FH approximation, Eq. (S4) resulting in:

$$\begin{aligned}\beta N_{av}{}^{-1}\mu_C&=(1-\nu)\phi_S+\ln\phi_C+\nu\chi\phi_S^2\\ \beta N_{av}{}^{-1}\mu_S&=\ln\phi_S+\left(1-\frac{1}{\nu}\right)\phi_C+\chi\phi_C^2\end{aligned} \tag{S9}$$

By using the multinomial theorem, the reduced grand canonical partition function is,

$$\Gamma\left(M\ ,V,\mu_W,\mu_G\right)=\frac{\lambda_S^{mM}}{M\ !}\psi^M \tag{S10}$$

where $\psi=\sum_{i=0}^{m}q(i)\exp(i\cdot\beta\cdot\Delta\mu)$, and $\Delta\mu=\mu_C-\mu_S$.

Finally, the adsorption entropy and energy are calculated using the appropriate derivatives of the grand canonical partition function, resulting in:

$$\frac{\Delta S}{M}=k\left[\ln\psi\lambda_S^m-\frac{m\mu_S}{kT}+\frac{1}{\psi}\sum_{i=0}^{m}q(i)\delta^i\Omega(i)\right] \tag{S11}$$

$$\frac{\Delta E}{M}=kT\left[\frac{\mu_S}{kT}\left(m-\frac{1}{\psi}\sum_{i=0}^{m_s}i\cdot q(i)\cdot\delta^i\right)+\frac{\mu_C}{kT}\left(\frac{1}{\psi}\sum_{i=0}^{m}i\cdot q(i)\cdot\delta^i\right)+\frac{\sum_{i=0}^{m}q(i)\cdot\delta^i\cdot\Omega(i)}{\psi}-\frac{m\mu_S}{kT}\right] \tag{S12}$$

where $\Omega(i)=\beta\left(\Delta h-i\cdot\Delta\mu\right)$. The adsorption free energy is calculated using the relation $\Delta A=\Delta E-T\Delta S$. The system is essentially incompressible, i.e., $\Delta(PV)=0$ such that $\Delta E=\Delta H$ and $\Delta A=\Delta G$.

Source of Model's Parameters

Excluded volume, ν . The ratio of the partial-molar volume of cosolute to solvent, $\nu=\bar{V}_C/\bar{V}_S$, describes the exclusion from the protein surface through the entropic contribution to the bulk and surface free energies, Eqs. (S1) and (S3). The entropic limit of the Asakura and Oosawa model (AOM) (Asakura et al. 1954; Asakura et al. 1958) is recovered when χ, ε, and their enthalpic and entropic contribution are set to 0.

We derive the excluded-volume parameter, ν, from PEG density (ρ) measurements (Ambrosone et al. 1996; Gonzalez-Tello et al. 1994; Muñoz et al. 2018). Fig. S5 shows molar volume, $\bar{V} = \rho^{-1}$, plotted against mole fraction, X_C. The relationship is linear over our concentration range, i.e., $\bar{V}_S$ and $\bar{V}_C$ are constant. Therefore, ν can be extracted by extrapolating the data to the appropriate limits: $\bar{V}_S = \lim_{X_C \to 0} \bar{V}$ and $\bar{V}_C = \lim_{X_C \to 1} \bar{V}$.

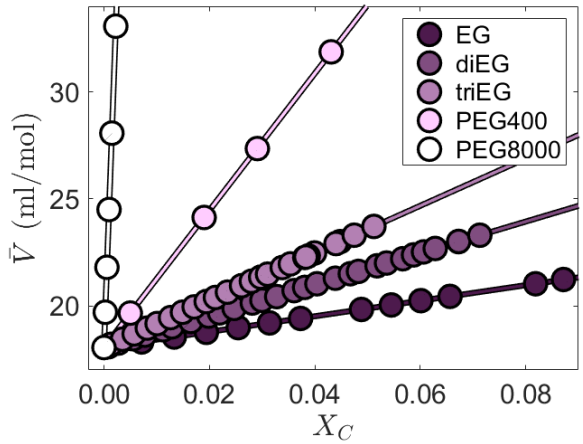

Figure S5. Molar volumes of aqueous PEG solutions as a function of mole fraction for different PEG sizes (small, EG, diEG, and triEG; medium, PEG400; and large, PEG8000) at ambient temperature.

Flory-Huggins (FH) solute-solvent interaction parameter, χ. The interaction between cosolute and solvent is described by χ, which accounts for the deviation from ideality of the solute-solvent mixture. Values of χ for non-volatile solutes like PEGs are extracted from water activity (a_W) measurements. The water activities in the presence of triEG (Table. S2), PEG400 (Table. S3), and PEG8000 (Table. S4) are measured using the dew point sensor of an AQUALAB 4TE water activity meter. Aqueous PEG solutions of up to 50 weight % are prepared gravimetrically. The meter is calibrated with standard salt solutions, and the sample chamber inner temperature is set in the range $15 - 45°C$. The sample size is $3\,mL$.

The osmotic pressure is calculated from the water activity using

$$\Pi = -\frac{1}{\bar{V}_S} \ln a_W \qquad \text{(S13)}$$

Fig S6. Shows the scaled osmotic pressure, $\Pi \bar{V}_S / kT$, for PEG400 and PEG8000 as a function of PEG volume fraction (ϕ_{PEG}), with fits to the expression derived from the model for cosolute exclusion from which χ can be extracted using

$$\frac{\Pi \bar{V}_S}{kT} = -\left[\ln\left(1-\phi\right) + \left(1-\frac{1}{\nu}\right)\phi + \chi\phi^2 \right] \quad \text{(S14)}$$

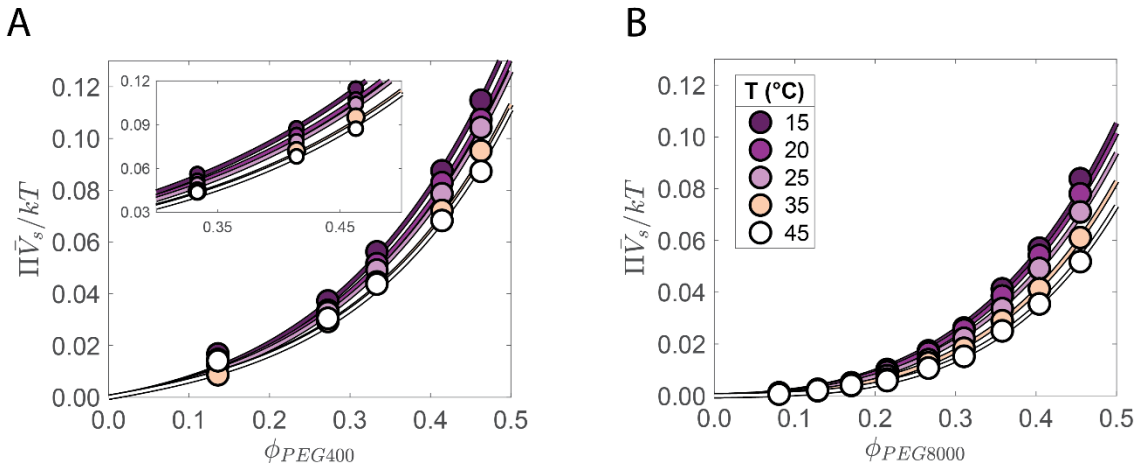

Figure S6. Normalized osmotic pressure as functions of volume occupancy and temperature for **(A)** PEG400 and **(B)** PEG8000. Curves are fits to the mean-field model.

χ for EG and diEG cannot be measured using the dew point method because of their high vapor pressures. Instead, the values were extracted from vapor pressure data Fig. S7 (Fujita et al. 2011; MEGlobal 2019a; MEGlobal 2019b).

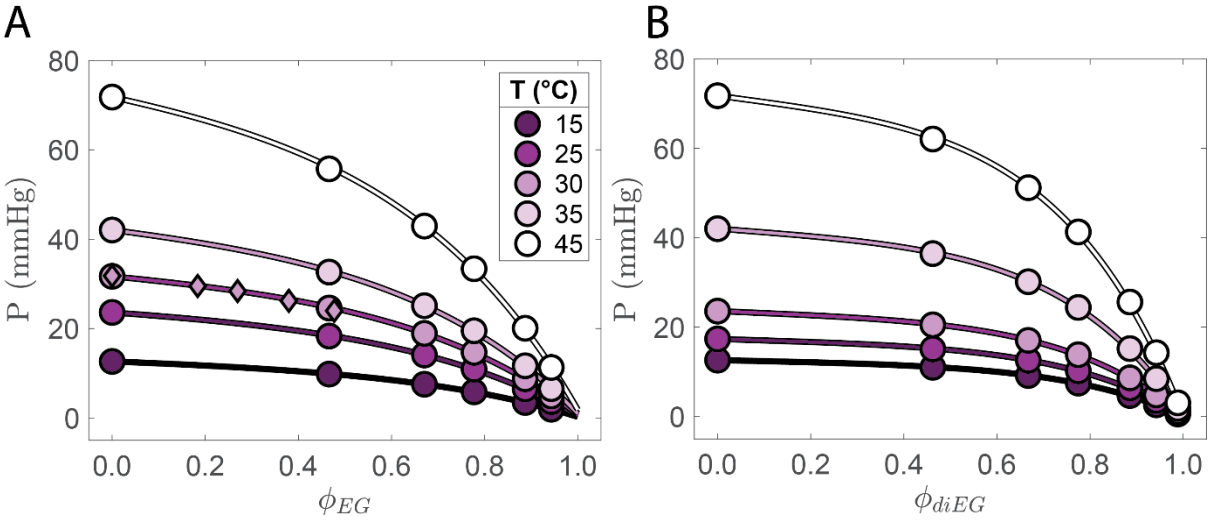

Figure S7. (A) EG and **(B)** diEG vapor pressure at different temperatures. Curves are fits to the mean-field model. Vapor pressures from MEGlobal and Fujita et al. are shown as circles and diamonds, respectively (Fujita and Kikuchi 2011; MEGlobal 2019a; MEGlobal 2019b).

Values of χ for EG and diEG are extracted from fits of the experiment-based vapor pressure to

$$P = P_S^{pure} e^{\frac{\mu_S}{kT}} + P_{EG/DiEG}^{pure} e^{\frac{\mu_{EG/DiEG}}{kT}} \quad \text{(S15)}$$

(Fig. S7), where the chemical potentials μ_S and $\mu_{EG/DiEG}$ are derived from FH theory for the bulk mixture Eq. (S9).

The validity of the χ values was verified by using water activity data from boiling point elevation (ebullioscopy) (Chouireb et al. 2018). A small difference between methods is observed for EG at higher concentrations, which is expected because of the elevated temperature at which the activity is measured ebullioscopically, resulting in a higher value of χ. For all cosolutes, we find $\chi > 0$ (Table. S5), indicating a net solvent-cosolute interaction that is less attractive than in the ideal solution.

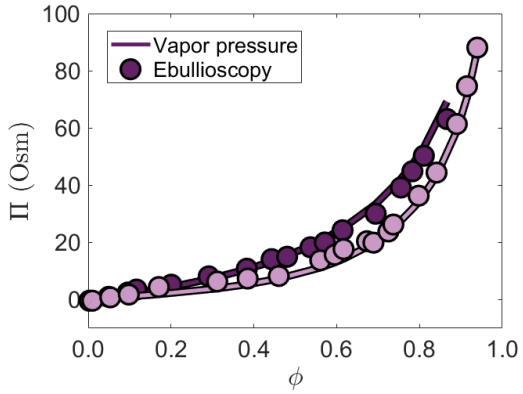

Figure S8. EG (purple) and diEG (pink) osmotic pressure derived from vapor pressure (full line) and ebullioscopy (circles) at $298\ K$.

Finally, the enthalpic and entropic contributions to the FH parameter, $\chi = \chi_H - \chi_{TS}$, are extracted by a van 't Hoff analysis, wherby the slope of the χ *-versus-* T^{-1} plot is $T \cdot \chi_H$ (Fig. S9). We find that the entropic contribution is repulsive ($\chi_{TS} < 0$) whereas the enthalpic contribution is attractive ($\chi_H < 0$), such that there is a net non-ideal repulsion because $\chi_{TS} < \chi_H$ (Table. S5).

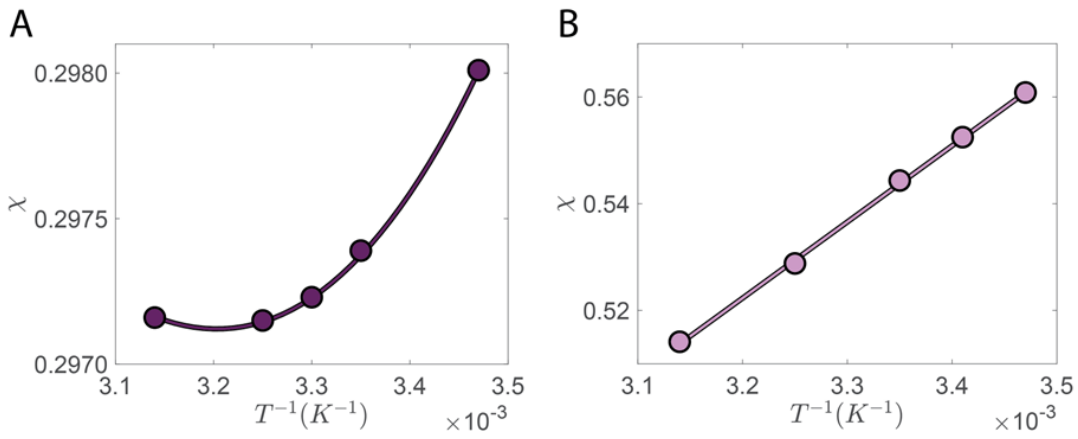

Figure S9. FH parameters for **(A)** EG and **(B)** diEG as function of inverse temperature. Fits to 2nd- and 1st-order polynomials, respectively, are shown.

Protein domain scaling. To fit $\Delta\Delta G_U^{\circ'}$, the experiment-based values of a, the linear dimension of the protein domain (Fig. 3 of main text) were interpolated using Padé fits of the form: $a=\left(A_0+A_1\phi\right)/\left(1+B_1\phi\right)$, for the cases of for $\varepsilon=0$ and $\varepsilon<0$. The resulting a fits for $\varepsilon=0$ were used to best fit the experimental $\Delta\Delta G_U^{\circ'}$ versus PEG concentration at $25\,^{\circ}C$, and are shown in Fig. 4 A and B in the main text.

Moreover, Fig. S10 shows the scaling behavior of a in presence of PEG400 and PEG8000, where the chemical interaction parameter $\varepsilon=-0.08$, which corresponds to net attractive interactions. As in the case of no chemical interaction ($\varepsilon=0$, Fig. 3D in the main text), the protein domain scales weakly with concentration for medium-sized PEGs. For larger PEG8000, the scaling of a conforms to the de-Gennes scaling law.

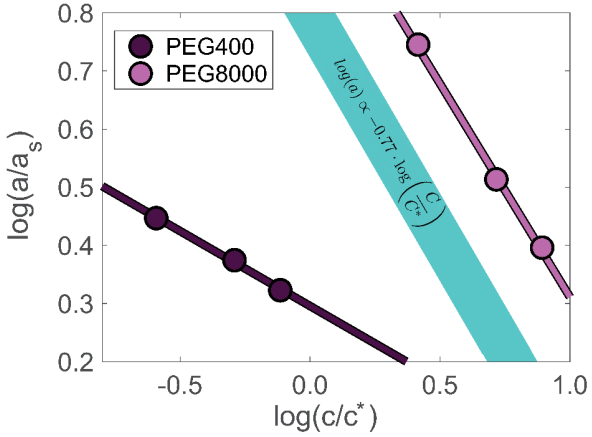

Figure S10. Protein domain size scaling for net attractive chemical interactions, $\varepsilon=-0.08$. The scaling is shown in a log-log plot of normalized a with normalized mass concentration.

Tables:

Table S1. Parameters determined from fits of stability ($\Delta G^{\circ'}$) to the integrated Gibbs–Helmholtz equation at varying PEG concentrations. Uncertainties (in brackets) determined from 95% confidence intervals.

	$\Delta H^{\circ'}_{Ts}\ (kcal/mol)$	$\Delta H^{\circ'}_{Tm}(kcal/mol)$	$Ts(K)$	$Tm(K)$
		$300\,g/L$		
Buffer	$1.01(0.03)$	$24.10(0.04)$	$287(1)$	$312.8(0.4)$
EG	$3.00(0.02)$	$43(2)$	$271(2)$	$315(1)$
diEG	$2.9(0.4)$	$42(3)$	$271(3)$	$313(1)$
triEG	$2.4(0.2)$	$38(2)$	$273(2)$	$311.7(0.5)$
tetraEG	$2.60(0.02)$	$39(2)$	$270(2)$	$209.8(0.4)$
PEG400	$2.70(0.05)$	$40(4)$	$270(4)$	$311(1)$
PEG600	$2.4(0.2)$	$38(1)$	$271(1)$	$310.0(0.4)$
PEG1000	$2.4(0.3)$	$38(2)$	$270(3)$	$311(1)$
PEG3350	$2.5(0.2)$	$39(1)$	$273(2)$	$312.0(0.4)$
PEG8000	$2.5(0.1)$	$39(1)$	$272(1)$	$311.9(0.3)$
PEG12000	$2.6(0.4)$	$39(3)$	$272(3)$	$312(1)$
PEG20000	$2.5(0.5)$	$39(4)$	$272(4)$	$312(1)$
PEG35000	$2.5(0.3)$	$39(2)$	$271(3)$	$311(1)$
		$200\,g/L$		
EG	$2.5(0.1)$	$39(1)$	$275(1)$	314.4 (0.5)
diEG	$2.4(0.1)$	$38(1)$	$274(1)$	$312(1)$
triEG	$2.2(0.1)$	$36(1)$	$275(1)$	$311(1)$
tetraEG	$2.1(0.1)$	$35.6(0.5)$	$275(1)$	$310.7(0.4)$
PEG400	$2.1(0.1)$	$36(1)$	$275(1)$	$311(1)$
PEG600	$2.1(0.1)$	$35(1)$	$274(1)$	$309.8(0.5)$
PEG1000	$2.2(0.1)$	$36(1)$	$274(1)$	$311(1)$
PEG3350	$2.1(0.2)$	$36(1)$	$276(2)$	$312(1)$
PEG8000	$2.1(0.1)$	$36(1)$	$276(1)$	$312(1)$
PEG12000	$2.3(0.2)$	$38(2)$	$274(2)$	$312(1)$
PEG20000	$2.1(0.1)$	$36(1)$	$276(1)$	$312(1)$
PEG35000	$2.2(0.2)$	$37(1)$	$275(2)$	$312(1)$

		$100\,g/L$		
EG	$1.8(0.1)$	$31(1)$	$280(1)$	$315(1)$
diEG	$1.7(0.1)$	$31(1)$	$280(1)$	$314(1)$
triEG	$1.6(0.1)$	$30(1)$	$279(2)$	$313(1)$
tetraEG	$1.6(0.1)$	$30(1)$	$279(1)$	$313(1)$
PEG400	$1.5(0.1)$	$28(1)$	$280(1)$	$312(1)$
PEG600	$1.5(0.1)$	$28(1)$	$280(1)$	$312(1)$
PEG1000	$1.5(0.1)$	$28(1)$	$280(1)$	$312(1)$
PEG3350	$1.5(0.1)$	$28(1)$	$281(1)$	$313(1)$
PEG8000	$1.5(0.1)$	$28(1)$	$281(1)$	$313(1)$
PEG12000	$1.5(0.1)$	$28(1)$	$281(1)$	$313(1)$
PEG20000	$1.5(0.1)$	$28(1)$	$281(1)$	$313(1)$
PEG35000	$1.5(0.1)$	$29(1)$	$281(1)$	$313(1)$
		$50\,g/L$		
EG	$1.39(0.06)$	$27.8(0.6)$	$283(1)$	$313.2(0.5)$
diEG	$1.36(0.09)$	$27.6(0.9)$	$284(1)$	$314(1)$
triEG	$1.33(0.04)$	$27.2(0.4)$	$283(1)$	$313.4(0.4)$
tetraEG	$1.23(0.07)$	$26.1(0.7)$	$284(1)$	$313(1)$
PEG1000	$1.25(0.05)$	$26.3(0.5)$	$284(1)$	$312.8(0.5)$
PEG12000	$1.21(0.05)$	$25.9(0.6)$	$285(1)$	$313(1)$
		$25\,g/L$		
EG	$1.17(0.03)$	$25.50(0.04)$	$285(1)$	$313.6(0.2)$
diEG	$1.1(0.6)$	$25.00(0.07)$	$286(1)$	$314(1)$
triEG	$1.1(0.3)$	$25.0(0.3)$	$286(1)$	$313.4(0.3)$
tetraEG	$1.11(0.07)$	$24.8(0.8)$	$285(1)$	$313(1)$
PEG1000	$1.11(0.04)$	$24.8(0.7)$	$286(1)$	$313.2(0.4)$
PEG12000	$1.06\ (0.05)$	$24.2(0.6)$	$286(1)$	$313(1)$

Table S2. ^{19}F chemical shift perturbation. Uncertainties (in brackets) denote the standard deviation of the mean from triplicate experiments.

Cosolute	Folded	Unfolded
	25 g/L	
EG	0.048 (0.009)	0.023 (0.004)
diEG	0.07 (0.01)	0.012 (0.005)
triEG	0.071 (0.006)	0.023 (0.002)
tetraEG	0.05 (0.01)	0.011 (0.006)
PEG1000	0.036 (0.005)	0.012 (0.002)
PEG12000	0.033 (0.006)	0.01 (0.002)
	50 g/L	
EG	0.09 (0.01)	0.038 (0.008)
diEG	0.11 (0.01)	0.035 (0.006)
triEG	0.113 (0.005)	0.043 (0.002)
tetraEG	0.087 (0.006)	0.027 (0.006)
PEG1000	0.052 (0.006)	0.025 (0.002)
PEG12000	0.045 (0.005)	0.017 (0.002)
	100 g/L	
EG	0.179 (0.009)	0.077 (0.003)
diEG	0.22 (0.01)	0.082 (0.001)
triEG	0.20 (0.01)	0.08 (0.002)
tetraEG	0.16 (0.01)	0.071 (0.001)
PEG400	0.110 (0.009)	0.053 (0.001)
PEG600	0.09 (0.01)	0.048 (0.001)
PEG1000	0.08 (0.01)	0.044 (0.001)
PEG3350	0.06 (0.01)	0.039 (0.002)
PEG8000	0.14 (0.01)	0.115 (0.002)
PEG12000	0.06 (0.01)	0.036 (0.002)
PEG20000	0.05 (0.01)	0.034 (0.001)
PEG35000	0.06 (0.01)	0.034 (0.002)

	200 g/L	
EG	0.32 (0.01)	0.144 (0.009)
diEG	0.43 (0.02)	0.15 (0.009)
triEG	0.54 (0.02)	0.138 (0.009)
tetraEG	0.42 (0.04)	0.124 (0.009)
PEG400	0.50 (0.02)	0.08 (0.02)
PEG600	0.27 (0.03)	0.083 (0.009)
PEG1000	0.29 (0.05)	0.085 (0.009)
PEG3350	0.24 (0.02)	0.07 (0.01)
PEG8000	0.24 (0.02)	0.07 (0.01)
PEG12000	0.19 (0.02)	0.06 (0.01)
PEG20000	0.21 (0.01)	0.07 (0.01)
PEG35000	0.22 (0.02)	0.06 (0.01)
	300 g/L	
EG	0.55 (0.03)	0.247 (0.004)
diEG	0.66 (0.03)	0.249 (0.006)
triEG	0.73 (0.04)	0.234 (0.005)
tetraEG	0.71 (0.03)	0.205 (0.007)
PEG400	0.8 (0.1)	0.164 (0.004)
PEG600	0.57 (0.06)	0.136 (0.006)
PEG1000	0.57 (0.07)	0.136 (0.006)
PEG3350	0.49 (0.03)	0.123 (0.004)
PEG8000	0.44 (0.03)	0.112 (0.003)
PEG12000	0.47 (0.03)	0.113 (0.004)
PEG20000	0.46 (0.03)	0.115 (0.004)
PEG35000	0.46 (0.03)	0.114 (0.008)

Table S3. Water activities in of triEG solutions. Standard deviation in brackets is derived from at least three measurements.

$m\,(mol/kg)$	a_W				
	$15°C$	$20°C$	$25°C$	$35°C$	$45°C$
1.177	0.9751(0.0005)	0.9762(0.0002)	0.9785(0.0002)	0.9763(0.0004)	0.9765(0.0003)
1.664	0.968(0.001)	0.9664(0.0003)	0.9684(0.0001)	0.9674(0.0007)	0.9672(0.0003)
2.208	0.9559(0.0003)	0.9535(0.0007)	0.9548(0.0004)	0.9549(0.0002)	0.9563(0.001)
2.857	0.9401(0.0004)	0.9396(0.0006)	0.9405(0.0005)	0.9410(0.0005)	0.9441(0.0007)
3.576	0.9201(0.0004)	0.9220(0.0003)	0.9246(0.0003)	0.9257(0.0004)	0.9310(0.0001)
4.430	0.8987(0.0001)	0.9007(0.0004)	0.9048(0.0003)	0.9077(0.0002)	0.9140(0.0002)
5.453	0.8730(0.0003)	0.8765(0.0004)	0.8810(0.0001)	0.8857(0.0006)	0.8926(0.0003)
6.660	0.8451(0.0008)	0.8490(0.0004)	0.8540(0.0002)	0.8610(0.0004)	0.8686(0.0003)

Table S4. Water activities of PEG400 solutions. Standard deviation in brackets is derived from at least three measurements.

$m\,(mol/kg)$	a_W				
	$15°C$	$20°C$	$25°C$	$35°C$	$45°C$
0.234	0.990(0.002)	0.991(0.002)	0.9916(0.0002)	0.988(0.009)	0.991(0.002)
0.467	0.983(0.002)	0.985(0.002)	0.9876(0.0005)	0.9913(0.0005)	0.986(0.003)
1.113	0.963(0.004)	0.9669(0.0004)	0.968(0.001)	0.9711(0.0006)	0.970(0.002)
1.489	0.945(0.005)	0.950(0.002)	0.9520(0.0008)	0.956(0.001)	0.957(0.001)
2.108	0.916(0.007)	0.9204(0.0004)	0.9243(0.0009)	0.9303(0.0004)	0.933(0.002)
2.573	0.89(0.01)	0.8982(0.0006)	0.9010(0.0003)	0.9091(0.0006)	0.916(0.004)
3.027	0.87(0.01)	0.8753(0.0006)	0.8797(0.0005)	0.890(0.001)	0.899(0.005)
4.268	0.83(0.02)	0.8367(0.0006)	0.8427(0.0002)	0.855(0.001)	0.867(0.007)

Table S5. Water activities of PEG8000 solutions. Standard deviation in brackets is derived from at least three measurements.

$m\,(mol/kg)$	a_W				
	$15°C$	$20°C$	$25°C$	$35°C$	$45°C$
0.013	0.9989(0.0002)	0.9991(0.0003)	0.9993(0.0001)	0.9990(0.0004)	0.9994(0.0005)
0.022	0.9978(0.0002)	0.9981(0.0005)	0.9976(0.0009)	0.9975(0.0005)	0.9979(0.0004)
0.031	0.9954(0.0002)	0.995(0.002)	0.9954(0.0008)	0.9960(0.0007)	0.9959(0.0003)
0.041	0.9900(0.0007)	0.9908(0.001)	0.9923(0.0007)	0.9936(0.0009)	0.9942(0.0004)
0.054	0.9828(0.0002)	0.9836(0.0002)	0.9862(0.0005)	0.9874(0.0002)	0.9894(0.0003)
0.068	0.9742(0.0007)	0.9749(0.0001)	0.97805(0.0006)	0.9819(0.0001)	0.9849(0.0001)
0.084	0.9596(0.0003)	0.9622(0.0001)	0.9669(0.0003)	0.9715(0.0005)	0.9753(0.0003)
0.102	0.9446(0.0002)	0.9472(0.0001)	0.9520(0.0004)	0.9596(0.0002)	0.9652(0.0001)
0.126	0.9196(0.0008)	0.9250(0.0002)	0.9315(0.0004)	0.9408(0.0001)	0.9495(0.0004)

Table S6. Models' parameters from binary mixture measurements.

Cosolute	χ	$\chi\left(kcal\cdot L^{-1}\right)$	χ_{TS}	$\chi_{TS}\,(kcal\cdot L^{-1})$	ν [c]	$c^*\,(g/L)$
EG	0.30	9.85	–3.98	–131	3.01	-
diEG	0.54	17.7	–0.93	–30.5	5.07	-
triEG	0.29	9.52	–1.62	–53.2	7.11	-
PEG400	0.38	12.5	–2.02	–66.3	18.7	390
PEG1000[a]	0.38	12.5	–2.02	–66.3	47.3	187
PEG3350[b]	0.40	13.1	–1.75	–57.4	156	74.1
PEG8000	0.40	13.1	–1.75	–57.4	371	38.4
PEG12000[b]	0.40	13.1	–1.75	–57.4	554	28.3
PEG20000[b]	0.40	13.1	–1.75	–57.4	910	19.3

[a] from PEG400 measurements

[b] from PEG8000 measurements

[c] ν, ratio of cosolute to water (0.018 L/mol) partial molar volumes

Table S7. Model chemical interaction parameters.

Cosolute	ε	ε $\left(kcal \cdot mol^{-1} \cdot nm^{-2}\right.$	ε_{TS}	ε_{TS} $\left(kcal \cdot mol^{-1} \cdot nm^{-2}\right)$	Δg	Δg $\left(\text{kcal} \cdot \text{mol}^{-1}\right)$	Δs	Δs $\left(\text{kcal} \cdot \text{mol}^{-1}\right)$
EG	–0.082	–0.51			–1.89	–1.12	1.15	0.682
diEG	–0.120	–0.74			–2.79	–1.65	–2.44	–1.45
triEG	–0.180	–1.11			–5.53	–3.28	–4.00	–2.37
PEG400								
PEG1000			0.60	3.7				
PEG3350	≤ 0							
PEG8000								
PEG12000								
PEG20000								

References

1. Ambrosone L, Sartorio R, Vescio A, Vitagliano V (1996) Volumetric Properties of Aqueous Solutions of Ethylene Glycol Oligomers at 25 °C. J Chem Soc, Faraday Trans 92:1163-1166.
2. Asakura S, Oosawa F (1954) On Interaction between Two Bodies Immersed in a Solution of Macromolecules. J Chem Phys 22:1255-1256.
3. Asakura S, Oosawa F (1958) Interaction between Particles Suspended in Solutions of Macromolecules. Journal of Polymer Science 33:183-192.
4. Chouireb N, Crespo EA, C. Pereira LM, Tafat-Igoudjilene O, Vega LF, Coutinho JAP, Carvalho PJ (2018) Measurement and Modeling of Isobaric Vapor–Liquid Equilibrium of Water + Glycols. J Chem Eng Data 63:2394-2401.
5. Fujita T, Kikuchi S (2011) Vapor Pressure of Aqueous Solutions of Ethylene Glycol. Trans Jpn Soc Refrig Air Cond Eng 6:183-186.
6. Gonzalez-Tello P, Camacho F, Blazquez G (1994) Density and Viscosity of Concentrated Aqueous Solutions of Polyethylene Glycol. J Chem Eng Data 39:611-614.
7. Gorensek-Benitez AH, Smith AE, Stadmiller SS, Perez Goncalves GM, Pielak GJ (2017) Cosolutes, Crowding, and Protein Folding Kinetics. J Phys Chem B 121:6527-6537.
8. Marsh JA, Neale C, Jack FE, Choy W-Y, Lee AY, Crowhurst KA, Forman-Kay JD (2007) Improved Structural Characterizations of the drkN SH3 Domain Unfolded State Suggest a Compact Ensemble with Native-Like and Non-Native Structure. J Mol Biol 367:1494-1510.
9. Maurer T, Kalbitzer HR (1996) Indirect Referencing Of31p And19f NMR Spectra. Journal of Magnetic Resonance, Series B 113:177-178.
10. MEGlobal. Diethylene Glycol Product Guide. (2019a).
11. MEGlobal. Ethylene Glycol Product Guide. (2019b).
12. Muñoz MM, Tinjacá DA, Jouyban A, Martínez F, Acree Jr WE (2018) Volumetric Properties of {PEG 200 (or 300)(1) + Water (2)} Mixtures at Several Temperatures and Correlation with the Jouyban–Acree Model. Phys Chem Liq 56:100-109.
13. Sapir L, Harries D (2015) Macromolecular Stabilization by Excluded Cosolutes: Mean Field Theory of Crowded Solutions. J Chem Theory Comput 11:3478-3490.
14. Senske M, Smith AE, Pielak GJ (2016) Protein Stability in Reverse Micelles. Angew Chem Int Ed Engl 55:3586-3589.
15. Smith AE, Zhou LZ, Gorensek AH, Senske M, Pielak GJ (2016) In-Cell Thermodynamics and a New Role for Protein Surfaces. Proc Natl Acad Sci U S A 113:1725-1730.
16. Stadmiller SS, Gorensek-Benitez AH, Guseman AJ, Pielak GJ (2017) Osmotic Shock Induced Protein Destabilization in Living Cells and Its Reversal by Glycine Betaine. J Mol Biol 429:1155-1161.
17. Stadmiller SS, Pielak GJ (2018) Enthalpic Stabilization of an SH3 Domain by D_2O. Protein Sci 27:1710-1716.
18. Thole JF, Fadero TC, Bonin JP, Stadmiller SS, Giudice JA, Pielak GJ (2021) Danio rerio Oocytes for Eukaryotic in-Cell NMR. Biochemistry 60:451-459.